Int. J. Heat Mass Transfer. Vol. 31, No. 2, pp. 429–440, 1988
Printed in Great Britain

0017–9310/88 $3.00 + 0.00

Combined radiation and free convection heat transfer in a vertical channel with arbitrary wall emissivities

YUKIO YAMADA
Mechanical Engineering Laboratory, Tsukuba Science City, Ibaraki 305, Japan

(*Received* 1 *September* 1987)

Abstract—Analytical and experimental studies of combined radiation and free convection heat transfer in a vertical channel in an absorbing and emitting medium are conducted. A channel consisting of parallel plates is heated asymmetrically, rendering both the wall and gas radiation important. A set of fundamental equations is established using the exponential wide-band model and the gray-gas model with arbitrary wall emissivities. Numerical results are compared with experimental ones. Wall emissivities are found to have a major effect on the combined heat transfer in this study. The gray-gas model is shown to fail to predict the negative net absorption in a gas layer next to an insulated wall.

1. INTRODUCTION

COMBINED radiation, convection, and conduction heat transfer have been studied by many investigators in the past 30 years, and a considerable number of reports has been accumulated since radiation heat transfer has become more and more important in engineering applications where higher temperatures and higher designing accuracies are required to improve the performance of power systems. The radiation heat transfer mode can be classified into two cases: one with only wall radiation, and the other with both wall and gas radiation.

One of the classical studies of combined wall radiation and forced convection heat transfer was analytically conducted by Siegel and Perlmutter [1] to report the end effects of pipe flow. Heat transfer augmentation using wall radiation for asymmetrical heating or cooling of non-radiating gas flow in plane parallel or annular ducts was investigated by Keshock and Siegel [2] and Mori *et al.* [3]. This idea was employed to develop advanced high temperature heat exchangers with heat transfer performances that were greatly improved by wall radiation [4, 5]. In these papers, augmentation of heat transfer by radiating inserts both inside and outside of the tube was studied experimentally and analytically in detail. Combined free convection and wall radiation heat transfer was also investigated [6]. The analytical and experimental study made clear the effects of surface emissivities and other factors in a vertical plane parallel flow passage.

For cases including gas radiation in combined heat transfer, which is always very important for combustion and other engineering applications, many investigators have produced numerous papers. Viskanta [7, 8] presented extensive literature surveys on this subject. The radiative properties of the absorbing and emitting gases, which are strongly dependent on wave number, have been approximated by various models: the gray-gas model, sum-of-gray-gas model, box model, wide-band model, narrow-band model, and others. Cess *et al.* [9] compared the accuracies of the results obtained using some of these various models.

Many numerical studies using the gray-gas model [10–12] are found in the literature. But it is well known that its simplicity introduces large errors in the results. The simplest among the non-gray models is the box model, which was also found to lead to large errors by Cess *et al.* [9]. The sum-of-gray-gas model was proposed by Hottel and Sarofim [13] and was recently modified by Song and Viskanta [14] and named the spectral-group model, which was applied to solve a problem of combined radiation and turbulent forced convection in furnaces.

The narrow-band model requires gas radiative properties of the bands given with a 25 cm^{-1} spectral resolution, and at least 20 or 30 bands must be defined, resulting in a formidable computing time. The wide-band model reduces the number of bands markedly, to less than ten, thus also reducing the computing time significantly. The exponential wide-band model proposed by Edwards and Menard [15] has been widely used by many investigators because of its usefulness. Correlations for the band absorptance of the exponential wide-band model were given by Tien and Lowder [16] and others [17–19]. The validity of these correlations were tested and compared with each other by Tiwari [20]. Edwards *et al.* [17] verified that their exponential wide-band model predicts much more accurate radiative properties than the gray-gas model by studying radiation heat transfer in non-isothermal radiating gases. DeSoto [21] applied the exponential wide-band model to a problem of coupled radiation, conduction, and convection in the entrance region flow. It was predicted that there exists a radiation boundary layer where non-gray gas emits more radiation to cool gas than it absorbs from hot black walls. Habib and Greif [22] and Greif [23] presented experimental and analytical studies of combined radi-

NOMENCLATURE

A_s	slab band absorption
A^*	dimensionless band absorption
B	black body radiosity
b	channel width
c_p	specific heat
E_n	nth order exponential integral
Gr	Grashof number
g	acceleration constant
I	spectral radiation intensity
$\hat{I}$	total intensity at walls
i,j	mesh points in the X- and Y-direction, respectively
J	mesh number at wall 2
K	dimensionless parameter appearing in the equation of state
L, l	dimensionless and dimensional channel height
P, p	dimensionless and dimensional pressure
Pr	Prandtl number
Q, q	dimensionless and dimensional heat flux
Q_w, q_w	dimensionless and dimensional input heat flux at walls
R	gas constant
s	path length of radiation beam
T, t	dimensionless and dimensional temperature
U, u	dimensionless and dimensional longitudinal velocity
V, v	dimensionless and dimensional transverse velocity
X, x	dimensionless and dimensional longitudinal distance
Y, y	dimensionless and dimensional transverse distance.

Greek symbols

α_g	spectral absorptivity of gas
γ_E	Euler constant, 0.5772 ...
$\Delta\nu_s$	band width
ε	wall emissivity
κ	absorption coefficient of gray gas
λ	dimensionless thermal conductivity
μ	dimensionless viscosity
ν	wave number, or dimensionless kinematic viscosity
ρ	dimensionless density
τ_0	optical thickness of the channel
τ_b, τ_c	optical thicknesses of the channel defined by equations (43) and (44)
τ_g	band transmissivity
τ_H	optical depth at band head or center.

Subscripts

0	inlet or environment
1, 2	walls 1 and 2, respectively
b	black body
i	radiation incoming to walls
m	spectral window
n	band
o	radiation outgoing from walls
R	gas radiation.

Superscripts

+	forward radiation
−	backward radiation
⁻	dimensional physical property.

ation and convection heat transfer in a vertical cylinder with turbulent or laminar CO_2 flow. The results using the exponential wide-band model were shown to agree very well with the accurately measured radial temperature profiles. Hirano *et al.* [24] predicted the possibility of augmentation of heat transfer between hot radiating gas and cooling walls by inserting a radiating wall which absorbs radiation in the bands and emits radiation through the spectral windows to heat up the cooling walls. The analysis employed the exponential wide-band model because the gray-gas model completely fails to predict this phenomenon. Song and Viskanta [14] also mentioned this effect in a recent paper. Many other studies of the combined radiation and convection heat transfer [25–28] reported analytical results using the wide-band model. Most of the literature incorporating the wide-band model assume symmetric heating and/or cooling of radiating gases with black bounding walls. (Tiwari and Cess [29] reported results with non-black walls, but there is some doubt about their basic formulations.) This is because it is difficult to evaluate the optical path length of a beam after reflection at non-black walls using the wide-band model.

The narrow-band model has the capability of predicting combined radiation, convection, and conduction with more general conditions and higher accuracy than any other models. Gill and Goody [30] published a detailed experimental and analytical study of the effect of radiation on the onset of convection in ammonia contained between horizontal plates maintained at different temperatures. Their analysis employed the statistical narrow-band model for the radiating properties and also presented formulations allowing non-black wall conditions. The agreement of the numerical and experimental results was found to be excellent. Nichols [31] studied combined radiation and convection heat transfer both experimentally and analytically in detail. The analysis using the statistical narrow-band model reported the radiative gas effect on the turbulent forced convection at the entrance region in an annular passage. The predicted 4% increase in heat transfer coefficients was verified by precise experiments. These two pioneering works

more than 20 years ago assumed small temperature differences and developed approximate solution methods like perturbation for thin optical thicknesses. Very recently, Soufiani and Taine [32] presented a numerical study of combined radiation and laminar forced convection at high temperatures and for a wide range of optical thicknesses using the random statistical narrow-band model, achieved with the help of great advances in computers. In the study, the Curtis–Godson approximation was employed to account for the radiative properties of the non-isothermal gas, and the results for arbitrary wall emissivities were obtained by integration over the bands with a 25 cm^{-1} spectral resolution. However, the fundamental radiative properties of the narrow-band model which were given in the study were previously determined and collected during their former extensive investigations [33–35] through line-by-line calculation, and the numerical calculation is still time consuming even for modern computers.

Most of the above described literature are analytical studies, while only a limited number of reports present experimental results. This is mainly because of the difficulty in obtaining high temperatures and large optical path lengths which can generate observable gas radiation effects within a laboratory setting. Also, most papers assume black walls and symmetric heating or cooling in order to simplify the formulation including the radiosities at the walls.

This paper reports the analytical and experimental study of a combined radiation and free convection between vertical parallel plates with asymmetric heating. Gas radiation coexists with wall radiation, and wall emissivities are allowed to be arbitrary. One of the purposes of this study is to present formulations for these conditions using the exponential wide-band model with a key assumption. The assumption alleviates the difficulty of applying the wide-band model to cases with non-black wall conditions. The predictions by the wide-band model analysis are compared with the experimental results and also with the analytical results using the gray-gas model.

2. ANALYSIS OF COMBINED RADIATION AND FREE CONVECTION HEAT TRANSFER BETWEEN PARALLEL PLATES

2.1. *Governing equations*

Figure 1 shows the configuration to be analyzed in this study. Free convection is induced in the channel between two parallel plates 1 and 2, which are heated from the outside by constant heat fluxes q_{w1} and q_{w2}, respectively. Both the bottom and top ends of the channel are open to the environment with temperature t_0 and pressure p_0. The working fluid is a gray or non-gray radiating gas without scattering. The x-axis extends vertically upward from the bottom of plate 1, and the y-axis extends horizontally. The channel width b is very small compared with the height l, so that the radiation can be reasonably assumed to be

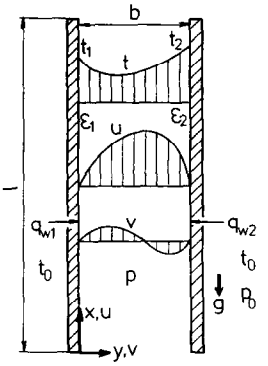

FIG. 1. Configuration of combined radiation and free convection.

one-dimensional; i.e. the variation of radiation is considered only in the y-direction. The difference of the heat inputs q_{w1} and q_{w2} makes the temperature profiles asymmetric, and the different plate temperatures t_1 and t_2 cause radiation exchange between the two plates with emissivities ε_1 and ε_2, respectively.

Fundamental mass, momentum, and energy equations for two-dimensional steady laminar free convection with radiation are well known [36] and the dimensionless expressions are

$$\frac{\partial(\rho U)}{\partial X}+\frac{\partial(\rho V)}{\partial Y}=0 \tag{1}$$

$$\rho U\frac{\partial U}{\partial X}+\rho V\frac{\partial V}{\partial Y}=-\frac{\mathrm{d}P}{\mathrm{d}X}+\frac{\partial}{\partial Y}\left(\mu\frac{\partial U}{\partial Y}\right)+\frac{1-\rho}{Q_{w1}+Q_{w2}} \tag{2}$$

$$\rho U\frac{\partial}{\partial X}(c_pT)+\rho V\frac{\partial}{\partial Y}(c_pT)=\frac{1}{Pr}\frac{\partial}{\partial Y}\left(\lambda\frac{\partial T}{\partial Y}\right)-\frac{1}{Pr}\operatorname{div}(Q_R). \tag{3}$$

The dimensionless variables and parameters defined in this section are summarized in the following:

$$X=\frac{x}{bGr},\quad Y=\frac{y}{b},\quad U=\frac{bu}{\bar{\nu}_0}Gr,\quad V=\frac{bv}{\bar{\nu}_0},\quad T=\frac{t}{t_0}$$

$$P=\frac{b^2(p-p_0)}{\bar{\rho}_0\bar{\nu}_0^2Gr^2},\quad Q=\frac{q}{\bar{\lambda}_0t_0}$$

$$\operatorname{div}(Q_R)=\frac{b^2}{\bar{\lambda}_0t_0}\operatorname{div}(q_R),\quad Gr=\frac{(q_{w1}+q_{w2})gb^4}{\bar{\lambda}_0\bar{\nu}_0^2t_0}$$

$$K=\frac{\bar{\nu}_0^2Gr^2}{Rt_0b},\quad Pr=\frac{\bar{\mu}_0\bar{c}_{p0}}{\bar{\lambda}_0},\quad \rho=\frac{\bar{\rho}}{\bar{\rho}_0},\quad \mu=\frac{\bar{\mu}}{\bar{\mu}_0}$$

$$\lambda=\frac{\bar{\lambda}}{\bar{\lambda}_0},\quad c_p=\frac{\bar{c}_p}{\bar{c}_{p0}}.$$

The boundary conditions for U, V, T, P are described by

$$U=6U_0(Y-Y^2),\ V=0,\ T=1,\ P=0;\ X=0$$

$$P=0;\ X=L$$

$$U=V=0;\ Y=0,1. \tag{4}$$

Here, a parabolic velocity profile with average U_0 is assumed at the inlet of the channel. The continuity of mass flow rate at every height X gives

$$\int_0^1 \rho U \, dY = U_0 \text{ const.} \tag{5}$$

The equation of state for an ideal gas is given by

$$KP = \rho T - 1. \tag{6}$$

The equation for div (q_R) and the energy balances at the two surfaces are required at this stage. But these equations depend on the model of gas radiation. In this paper, the exponential wide-band model by Edwards [37] and the gray-gas model are employed.

2.2. *Use of the exponential wide-band model*

One of the most useful and successful models for non-gray absorbing and emitting gases is the exponential wide-band model proposed by Edwards. But almost all of the previous works using Edwards' model have obtained results with the assumption of black surfaces because of the inherent difficulty of the wide-band model in the analysis for non-black surfaces [32].

The forward and backward spectral intensities I^+ and I^- at location s in local thermal equilibrium are described by

$$I_n^+(\nu, s) = I_{1n}(\nu) - [I_{1n}(\nu) - I_{b,n}(\nu, 0)]\alpha_{gn}(\nu; 0, s) + \int_0^s \alpha_{gn}(\nu; s', s) \frac{dI_b}{ds} ds' \tag{7}$$

$$I_n^-(\nu, s) = I_{2n}(\nu) - [I_{2n}(\nu) - I_{b,n}(\nu, s_0)]\alpha_{gn}(\nu; s, s_0) - \int_s^{s_0} \alpha_{gn}(\nu; s, s') \frac{dI_b}{ds} ds' \tag{8}$$

where n denotes the nth band, and I_1, I_2, and I_b are the spectral intensities at the two surfaces and of a black body, respectively. $\alpha_{gn}(s', s)$ is the spectral absorptivity of the gas column between the two locations s' and s. Now, by using the wide-band model of Edwards, equations (7) and (8) are integrated for slab geometry using the one-dimensional radiation assumption and also integrated by wave number within the range of the band width $\Delta\nu_{sn}$ which is the widest band width in the case considered

$$\pi I_{sn}^+(y) \cdot \Delta\nu_{sn} = \pi I_{1n} \cdot \Delta\nu_{sn} - [\pi I_{1n} - B(\nu_n, t_1)]A_{sn}(0, y) + \int_0^y A_{sn}(y', y) \frac{\partial B(\nu_n, t)}{\partial t} \cdot \frac{\partial t}{\partial y'} dy' \tag{9}$$

$$\pi I_{sn}^-(y) \cdot \Delta\nu_{sn} = \pi I_{2n} \cdot \Delta\nu_{sn} - [\pi I_{2n} - B(\nu_n, t_2)]A_{sn}(y, b) - \int_y^b A_{sn}(y, y') \frac{\partial B(\nu_n, t)}{\partial t} \cdot \frac{\partial t}{\partial y'} dy' \tag{10}$$

where subscript s denotes slab geometry, B is the spectral radiosity of a black body, and A_{sn} is the slab band absorptance. The band width $\Delta\nu_{sn}$ is obtained from

$$\Delta\nu_{sn} = \nu_{sn}(\text{upper limit}) - \nu_{sn}(\text{lower limit}) = \frac{A_{sn}(0, b)}{1 - \tau_{gsn}(0, b)}$$

$$\tau_{gsn}(0, b) = \frac{\tau_{Hn}(0, b)}{A_{sn}(0, b)} \frac{dA_{sn}(0, b)}{d\tau_{Hn}(0, b)} \tag{11}$$

where $\tau_{bsn}(0, b)$ is the transmissivity of the gas slab and $\tau_{Hn}(0, b)$ is the maximum optical depth at the band head. Equations (9) and (10) have been derived by employing an assumption that in the nth band the spectral profiles of the intensities at surfaces 1 and 2, I_{1n} and I_{2n}, are not so different from those of the black bodies at temperatures t_1 and t_2. This key assumption is valid when the optical thickness of the gas slab between the two surfaces is small. Because the distortions of the spectral intensity profiles of the bands emanating from one surface are acceptably small when the radiation reaches the other surface after absorption and emission by the optically thin gas slab. On the other hand, this assumption may be valid when the optical thickness is so large that the contribution of the surface emission is negligible [32].

The intensities at the mth spectral windows are expressed as follows:

$$\pi I_{sm}^+(y) \cdot \Delta\nu_{sm} = \int_{\Delta\nu_{sm}} \pi I_{1m} \, d\nu \tag{12}$$

$$\pi I_{sm}^-(y) \cdot \Delta\nu_{sm} = \int_{\Delta\nu_{sm}} \pi I_{2m} \, d\nu \tag{13}$$

where $\Delta\nu_{sm} = \Delta\nu_{sn}(\text{lower limit}) - \Delta\nu_{sn-1}(\text{upper limit})$. By adding the intensities for the bands and windows, the radiative heat fluxes q_R^+ and q_R^-, are expressed as

$$q_R^+(y) = \sum_m \pi I_{sm}^+(y) \cdot \Delta\nu_{sm} + \sum_n \pi I_{sn}^+(y) \cdot \Delta\nu_{sn} \tag{14}$$

$$q_R^-(y) = \sum_m \pi I_{sm}^-(y) \cdot \Delta\nu_{sm} + \sum_n \pi I_{sn}^-(y) \cdot \Delta\nu_{sn}. \tag{15}$$

Now, the intensities from the surfaces at the bands and windows are combined and expressed as $\pi\hat{I}_1$ and $\pi\hat{I}_2$

$$\pi\hat{I}_1 = \sum_m \int_{\Delta\nu_{sm}} \pi I_{1m} \, d\nu + \sum_n \pi I_{1n} \Delta\nu_{sn} \tag{16}$$

$$\pi\hat{I}_2 = \sum_m \int_{\Delta\nu_{sm}} \pi I_{2m} \, d\nu + \sum_n \pi I_{2n} \Delta\nu_{sn}. \tag{17}$$

Then, equations (14) and (15) are reduced to

$$q_R^+(y) = \pi\hat{I}_1 + \sum_n \left\{ [B(\nu_n, t_1) - \pi I_{1n}]A_{sn}(0, y) + \int_0^y A_{sn}(y', y) \frac{\partial B(\nu_n, t)}{\partial t} \cdot \frac{\partial t}{\partial y'} dy' \right\} \tag{18}$$

$$q_R^-(y) = \pi\hat{I}_2 + \sum_n \left\{[B(\nu_n, t_2) - \pi I_{2n}]A_{sn}(y, b) - \int_y^b A_{sn}(y, y')\frac{\partial B(\nu_n, t)}{\partial t}\cdot\frac{\partial t}{\partial y'}\,dy'\right\}. \quad (19)$$

Finally, div (q_R) is given by

$$\begin{aligned}\text{div}\,(q_R) &= \frac{dq_R(y)}{dy} = \frac{d}{dy}[q_R^+(y) - q_R^-(y)] \\ &= \sum_n \left\{[B(\nu_n, t_1) - \pi I_{1n}]\frac{\partial A_{sn}(0, y)}{\partial y}\right. \\ &\quad - [B(\nu_n, t_2) - \pi I_{2n}]\frac{\partial A_{sn}(y, b)}{\partial y} \\ &\quad + \frac{\partial}{\partial y}\left[\int_0^y A_{sn}(y', y)\frac{\partial B(\nu_n, t)}{\partial t}\cdot\frac{\partial t}{\partial y'}\,dy'\right. \\ &\quad \left.\left. + \int_y^b A_{sn}(y, y')\frac{\partial B(\nu_n, t)}{\partial t}\frac{\partial t}{\partial y'}\,dy'\right]\right\} \quad (20)\end{aligned}$$

πI_{1n} and πI_{2n} in the above equations are obtained by solving the following equations:

$$\pi I_{1n} = \varepsilon_{1n}B(\nu_n, t_1) + (1-\varepsilon_{1n})\pi I_{sn}^-(0) \quad (21)$$

$$\pi I_{2n} = \varepsilon_{2n}B(\nu_n, t_2) + (1-\varepsilon_{2n})\pi I_{sn}^+(b) \quad (22)$$

where ε_{1n} and ε_{2n} are the surface emissivities at the nth band. The surfaces are assumed to be diffusely emitting and reflecting, and also the surface emissivities are assumed not to vary with wave number within each band. $\pi I_{sn}^-(0)$ and $\pi I_{sn}^+(b)$ are given by equations (9) and (10). Now the heat balances at the surfaces are required. Consider the outgoing radiative fluxes from the surfaces, $q_{o,1}$ and $q_{o,2}$, the incoming fluxes to the surfaces, $q_{i,1}$ and $q_{i,2}$, and the net radiative fluxes q_1 and q_2. These fluxes are related by the following equations:

$$q_{o,1} = \varepsilon_1 R_b(0) + (1-\varepsilon_1)q_{i,1} \quad (23)$$

$$q_{o,2} = \varepsilon_2 R_b(b) + (1-\varepsilon_2)q_{i,2} \quad (24)$$

$$q_1 = q_{o,1} - q_{i,1} \quad (25)$$

$$q_2 = q_{o,2} - q_{i,2} \quad (26)$$

where ε_1 and ε_2 are the total emissivities of the surfaces, and R_b is the total black body radiosity; $R_b(0) = \sigma t_1^4$, $R_b(b) = \sigma t_2^4$. $q_{o,1}$, $q_{o,2}$, $q_{i,1}$ and $q_{i,2}$ are expressed as

$$q_{o,1} = \pi\hat{I}_1, \quad q_{o,2} = \pi\hat{I}_2 \quad (27)$$

$$q_{i,1} = q_R^-(0), \quad q_{i,2} = q_R^+(b). \quad (28)$$

Eliminating $q_{o,1}$, $q_{o,2}$, $q_{i,1}$ and $q_{i,2}$ from equations (23) to (28) gives the following two equations for the surface temperatures t_1 and t_2:

$$\sigma t_1^4 - \frac{q_1}{\varepsilon_1} = \sigma t_2^4 - \frac{1-\varepsilon_2}{\varepsilon_2}q_2 + Q_{R2} \quad (29)$$

$$\sigma t_2^4 - \frac{q_2}{\varepsilon_2} = \sigma t_1^4 - \frac{1-\varepsilon_1}{\varepsilon_1}q_1 + Q_{R1} \quad (30)$$

where

$$Q_{R1} = \sum_n \left\{[B(\nu_n, t_1) - \pi I_{1n}]A_{sn}(0, b) + \int_0^b A_{sn}(y', b)\frac{\partial B(\nu_n, t)}{\partial t}\cdot\frac{\partial t}{\partial y'}\,dy'\right\} \quad (31)$$

$$Q_{R2} = \sum_n \left\{[B(\nu_n, t_2) - \pi I_{2n}]A_{sn}(0, b) - \int_0^b A_{sn}(0, y')\frac{\partial B(\nu_n, t)}{\partial t}\cdot\frac{\partial t}{\partial y'}\,dy'\right\}. \quad (32)$$

The net radiative heat fluxes q_1 and q_2 are given by

$$q_1 = q_{w1} + \left(\lambda\frac{\partial t}{\partial y}\right)_{y=0} \quad (33)$$

$$q_2 = q_{w2} - \left(\lambda\frac{\partial t}{\partial y}\right)_{y=b}. \quad (34)$$

The seven unknowns p, ρ, u, v, t, t_1, and t_2 are obtained by solving the seven governing equations, equations (1)–(3), (5), (6), (29), and (30) with the auxiliary equations, equations (20)–(22), (33), and (34), and with the boundary conditions, equation (4).

2.3. *Use of the gray-gas model*

The assumption of one-dimensional radiation and the gray-gas model give the following equation for div (q_R):

$$\text{div}\,(q_R) = \frac{\partial q_R}{\partial y} = 2\kappa\left[2\sigma t^4 - \int_0^{\tau_0}\sigma t^4 E_1(|\tau-\xi|)\,d\xi - \pi I(0)E_2(\tau) - \pi I(\tau_0)E_2(\tau_0-\tau)\right]. \quad (35)$$

Here, κ and $\tau = \kappa y$ are the absorption coefficient and the optical thickness of the radiating gas, respectively, and σ is the Stefan–Boltzmann constant. $\tau_0 = \kappa b$ is the optical thickness of the channel, and $E_n(\tau)$ is the exponential attenuation function. The intensities $I(0)$ and $I(\tau_0)$ at the two surfaces are obtained by the following two equations:

$$\pi I(0) = \varepsilon_1\sigma t_{w1}^4 + 2(1-\varepsilon_1)\left[\pi I(\tau_0)E_3(\tau_0) + \int_0^{\tau_0}\sigma t^4 E_2(\xi)\,d\xi\right] \quad (36)$$

$$\pi I(\tau_0) = \varepsilon_2\sigma t_{w2}^4 + 2(1-\varepsilon_2)\left[\pi I(0)E_3(\tau_0) + \int_0^{\tau_0}\sigma t^4 E_2(\tau_0-\xi)\,d\xi\right] \quad (37)$$

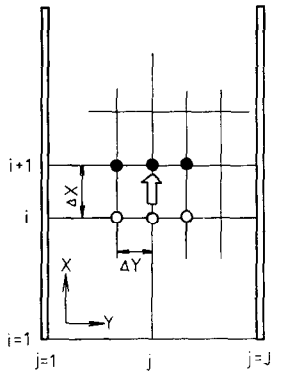

FIG. 2. Mesh points for finite difference equations.

Consideration of heat balances at the two surfaces gives

$$\sigma t_{w1}^4 - \frac{q_1}{\varepsilon_1} = \left(\sigma t_{w2}^4 - \frac{1-\varepsilon_2}{\varepsilon_2} q_2\right) \cdot 2E_3(\tau_0) + 2\int_0^{\tau_0} \sigma t^4 E_2(\xi)\,\mathrm{d}\xi \quad (38)$$

$$\sigma t_{w2}^4 - \frac{q_2}{\varepsilon_2} = \left(\sigma t_{w1}^4 - \frac{1-\varepsilon_1}{\varepsilon_1} q_1\right) \cdot 2E_3(\tau_0) + 2\int_0^{\tau_0} \sigma t^4 E_2(\tau_0 - \xi)\,\mathrm{d}\xi. \quad (39)$$

Now, the seven governing equations are equations (1)–(3), (5), (6), (38), and (39) with the five auxiliary equations, equations (33)–(37) and with the boundary conditions, equation (4).

2.4. *Method of calculation*

The numerical solution of the dimensionless governing equations is obtained by the marching method similar to that employed by Aung *et al.* [38]. The governing equations, equations (1)–(3), and (5), are replaced by implicit finite difference equations using the mesh points shown in Fig. 2. One hundred and one mesh points are used in the Y-direction. A progressively increasing step size is used in the X-direction, and the typical total step number is about 45.

The flow rate parameter U_0 is given initially, then the seven unknowns are numerically obtained at the next step to $X = 0$. T_1 and T_2 are obtained from equations (29) and (30), $T(Y)$ from equation (3), $U(Y)$ and P from equations (2) and (5), $\rho(Y)$ from equation (6), and finally $V(Y)$ from equation (1). Iteration continues until these unknowns converge at each step i, and then the calculation proceeds to the next step $i+1$. This marching procedure continues until the pressure at some step returns to the inlet pressure p_0 at the end of the channel. If the channel length is different from the desired one, another marching starts after adjusting the flow rate parameter U_0.

In calculation of T_1 and T_2, the temperature gradients at the two surfaces appearing in equations (33) and (34) are given by

$$\left(\lambda \frac{\partial T}{\partial Y}\right)_{Y=0} = \lambda_{j=1} \frac{-3T_1 + 4T_{j=2} - T_{j=3}}{2 \cdot \Delta Y} \quad (40)$$

$$\left(\lambda \frac{\partial T}{\partial Y}\right)_{Y=1} = \lambda_{j=J} \frac{T_{j=J-2} - 4T_{j=J-1} + 3T_2}{2 \cdot \Delta Y}. \quad (41)$$

Then equations (29) and (30) for the wide-band model are combined to give a linear equation for T_1 and T_2. Subsequently, equation (30) is reduced to a fourth-order polynomial of T_2 which is easily solved by the Newton–Raphson method.

For the gray-gas model, equations (38) and (39) can also be combined to give two fourth-order polynomials for T_1 and T_2.

The terms div (Q_R) in equation (3), Q_{R1} and Q_{R2} in equations (29) and (30), and the integrals in equations (38) and (39) are evaluated using the values of the previous iteration.

Pure carbon dioxide, CO_2, was used in the experiment as a radiating gas with the temperature range below 300°C. Therefore, only three major bands at 2.7, 4.3, and 15 μm are considered for the exponential wide-band model with the parameters given by Edwards [37]. Correlation (42) for the band absorption given by Edwards and Morizumi [39] is employed

$$A^* = \ln \tau_H + E_1(\tau_H) + \gamma_E \quad (42)$$

where A^* is a dimensionless band absorption. Also, the scaling for the band parameters to allow the temperature variation through the radiation path is incorporated in the numerical calculation, although the scalings are not necessarily required for the temperature range considered in the experiments of this study.

The optical thickness of the gray-gas slab is estimated by two methods. One is τ_b which is calculated from the gas emissivity ε_g obtained by the exponential wide-band model

$$1 - 2E_3(\tau_b) = \varepsilon_g = \frac{\sum_n A_{sn}(0, b) B(\nu_n, t_0)}{\sigma t_0^4}. \quad (43)$$

The other is τ_c which is estimated from the absorption coefficients κ given by Cess [40]. κ is correlated by equation (44) to be a linear function of temperature with its coefficients also varying linearly with pressure

$$\tau_c = b[164p_0 - 3.06 - (4.89 \times 10^{-2} p_0 + 4.78 \times 10^{-3}) t_0]. \quad (44)$$

When the gray-gas model is used in varying temperature fields, an adequate representative temperature should be taken to calculate the gray-gas optical thickness. In this study, the temperature of the environment was selected as representative since the temperature variation of the working gas in the experiments is less than 100°C.

Temperature dependence of three physical properties was also incorporated. They are given by equation (45) with the powers $a = 0.0096$, $b = 0.754$,

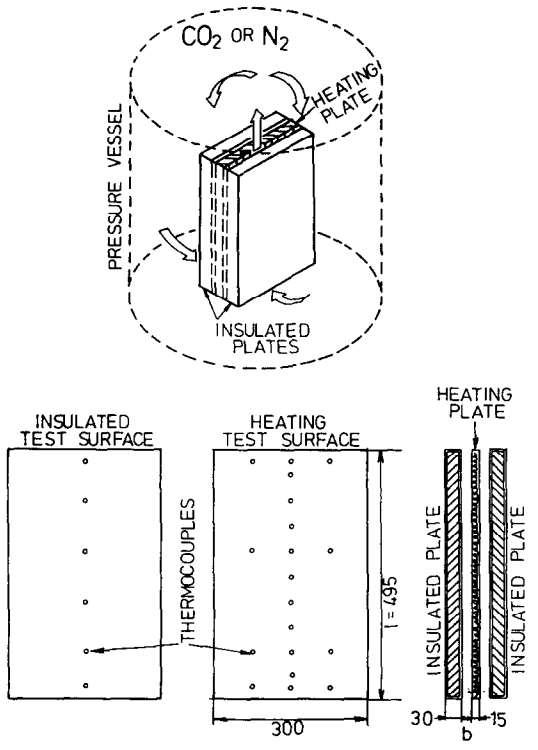

FIG. 3. Experimental apparatus.

$c = 0.841$ for nitrogen and $a = 0.338$, $b = 0.905$, $c = 1.359$ for carbon dioxide

$$c_p = T^a, \quad \mu = T^b, \quad \lambda = T^c. \tag{45}$$

3. EXPERIMENTAL APPARATUS AND METHOD

The experimental apparatus for combined radiation and free convection is shown in Fig. 3. A combination of an electric heating plate and two insulated plates was contained vertically in a pressure vessel. The heating plate was aligned between the two insulated plates, thus two plane-parallel channels of the same size were created. The channels were open to the environment at the top and bottom ends and had closed sides. The channel width was varied from 10 to 30 mm, which was less than one tenth of the plate width, providing satisfactory two-dimensionality of the channel and negligible side effect. The width and height of the three plates were 300 and 495 mm, respectively. The heating plate had electric heating wires embedded inside to provide uniform wall heat fluxes. The insulated plates consisted of 30 mm thick insulation with stainless steel covers. Measuring heat fluxes from the back surfaces of the insulated plates confirmed the negligible heat losses. Also, the heat flux difference between the two surfaces of the heating plate was measured to be less than 4%, confirming that the heat input to one channel was half of the total input. Then one channel was taken as the test channel for measuring temperatures and the other channel was considered to be a dummy to assure the symmetry to the heating plate. The test surface of the heating plate had 19 thermocouples embedded into the stainless steel cover plate, and the other dummy surface contained 8 thermocouples. Of the 19 thermocouples 11 were located on the vertical center line of the test surface, and 4 were located on the center line of the other surface. The maximum deviation of the surface temperatures in the horizontal direction was measured to be 2.6°C when the gas and center line surface temperatures were 53 and 78°C, respectively. This deviation was small enough to assure the temperature uniformity in the horizontal direction. Hence, only center line temperatures were employed in the following data reduction. The test insulated plate had 6 thermocouples on the center line of the test surface.

The surfaces of the plates were polished with #60 emery paper. In order to observe the effect of surface emissivities, experiments were conducted with all polished surfaces or all black painted surfaces. The total emissivity of the polished surface was given as 0.18, taken from the literature [41]. The total emissivities of the black painted surface were previously measured by the author [42] to give 0.8 at 50°C, 0.9 at 200°C, and increasing at higher temperatures.

The pressure vessel had a 500 mm i.d. and a 1000 mm maximum inside height, with the capability of being pressurized up to 0.8 MPa and heated up to 200°C. A coil of tube was contained at the inside top of the vessel, and a jacket surrounded the vessel sides to form an annular duct. Air at an appropriate temperature was forced to flow in the coil and the annular duct in order to control the gas temperature inside the vessel. Carbon dioxide or nitrogen was used as the working gas. Changing the pressure, channel width, and heat input gave the variations in the Grashof number and optical depth.

4. RESULTS OF ANALYSES AND EXPERIMENTS

4.1. *Non-radiating gas*

Before investigating the simultaneous wall and gas radiation effect in the combined radiation and free convection, a non-radiating gas was used as a working fluid to separate the wall radiation effect from the gas radiation effect. Figure 4 shows wall temperature variations for two cases using nitrogen at atmospheric pressure with a 10 mm channel width. Good agreement between the experimental and numerical results of the wall temperatures was observed except at the area close to the outlet. The temperature drops near the outlet were likely to be induced by undesirable inflows from the cold environment. This trend was observed in all of the experiments in this study. These two cases had the same conditions except for the surface emissivities. The total emissivities of the black painted surface were measured as 0.82 averaged over the temperature range in Fig. 4, while those of the polished surface were evaluated as 0.18, as previously

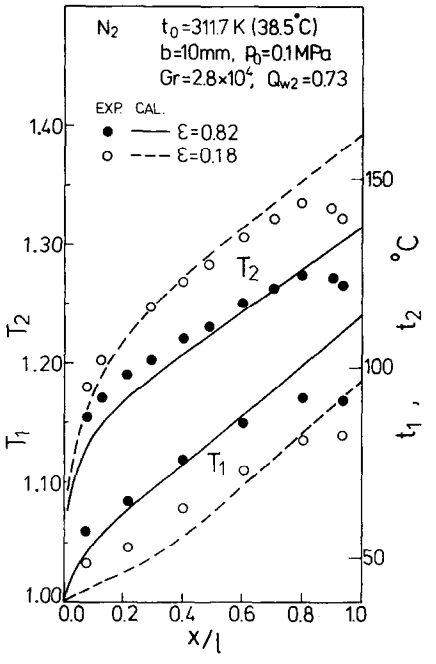

FIG. 4. Wall temperature profile in the flow direction for high and low emissivities using N_2.

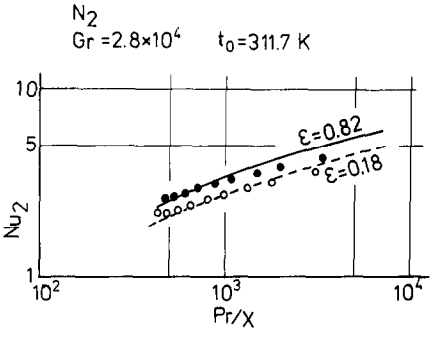

FIG. 5. Nu_2 variations for high and low emissivities using N_2.

mentioned. Because the heat transfer coefficients of free convection are small, radiation exchange between the two surfaces is comparable to free convection heat transfer even at a temperature of around 100°C. The net radiation heat flux from the heating surface occupied 46% of the total heat flux q_{w2} for $\varepsilon = 0.82$, and 22% for $\varepsilon = 0.18$. Thus, the free convection heat transfer from the heating surface is enhanced by the insulated surface. The Nusselt numbers at the heating surface Nu_2 defined by equation (46) are shown in Fig. 5

$$Nu_2 = \frac{bq_{w2}}{\lambda(t_2 - t_0)}. \quad (46)$$

The ratio of Nusselt numbers for $\varepsilon = 0.82$ to that for $\varepsilon = 0.18$ is numerically predicted to be 1.25. This ratio increases to a maximum of about 1.8 when the two limiting cases with $\varepsilon = 1.0$ and 0 are considered.

4.2. *Radiating gas*

Figure 6 shows experimental and numerical results of the wall temperatures using CO_2 as the working gas. Experimental results for high and low surface emissivities are shown by three curves obtained by numerical calculation. Solid lines have been obtained by the wide-band model, dotted lines by the gray-gas model with the optical depth given by equation (44) from Cess, and dotted-broken lines for non-radiating $CO_2(\tau_0 = 0)$. Curves by the gray-gas model with the optical depth based on the wide-band model, equation (43), are slightly different but indiscernible from the solid lines by the wide-band model. The agreement between the numerical and experimental results is better than that in Fig. 4 using N_2. Both the heating rates and the induced flow velocities for Figs. 4 and 6 are of the same order. Therefore, the reason why the agreement in Fig. 4 is not as good as in Fig. 6 is not clear. The emissivity and optical depth of the slab gas in Fig. 6 given by equation (43) are $\varepsilon_g = 0.088$ and $\tau_b = 0.049$, showing that the contribution of gas radiation is not dominant. Consequently, the effect of the surface emissivities has similar importance to the case using nitrogen. The ratio of Nu_2 for $\varepsilon = 0.82$ to that for $\varepsilon = 0.18$ is 1.34 from the calculation using the wide-band model. Nu_2 obtained by the wide-band model is compared with the experimental results in Fig. 7. Returning to Fig. 6, because of the thin optical thickness, the numerical wall temperature profiles obtained with different models for gas radiation are lying within a temperature range of ± 3°C, which is almost the same as the uncertainty in the measured wall temperatures. Therefore, it is difficult to state that the numerical results obtained by any one of the models agree perfectly. However, it is reasonable to

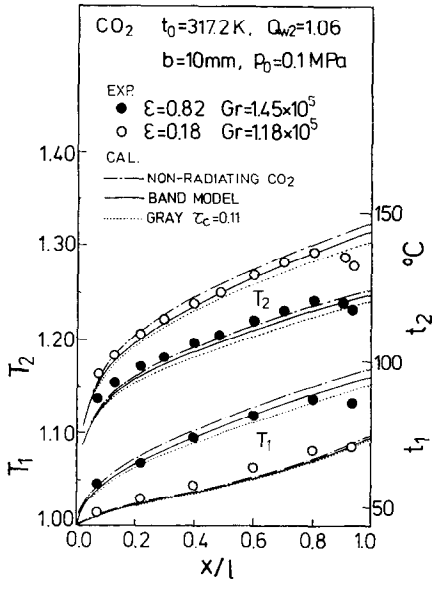

FIG. 6. Wall temperature profile in the flow direction for high and low emissivities using CO_2 with $b = 10$ mm and $p_0 = 0.1$ MPa.

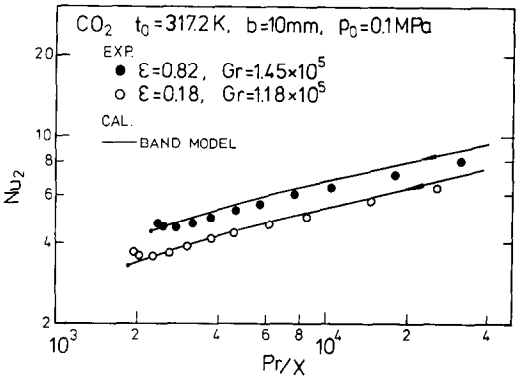

FIG. 7. Nu_2 variations for high and low emissivities using CO_2 with $b = 10$ mm and $p_0 = 0.1$ MPa.

conclude that the wide-band model is shown to give better agreement than any other models considered in this study. Also, it is shown by this figure that gas radiation lowers both the heating and insulated wall temperatures, and this lowering effect becomes larger as the optical thickness gets thicker.

The optical thickness $\tau_c = 0.11$ given by equation (44) is more than twice that of $\tau_b = 0.049$. The values of κ given by Cess are based on the data for the thin limit, and it is widely known that these values are not suitable to be extrapolated to thick gas since the properties of gas radiation are highly nonlinear with respect to gas thickness. This inadequacy of using equation (44) is further demonstrated by an example described later.

Figure 8(a) compares the numerical results of the gas temperature profiles for $\varepsilon = 0.82$ at $x/l = 0.917$ by the four different gas radiation properties: the wide-band model, the gray-gas model with two different optical depths τ_b and τ_c, and the non-radiative gas $\tau_0 = 0$. Gas absorption and emission flatten the temperature profiles within the gas. The hot portions near the surfaces emit radiation to reduce their temperatures, while the cold portion in the channel core absorbs radiation. This phenomenon is quantitatively described by the profiles of $-\text{div}\,(Q_R)$ shown in Fig. 8(b). Negative values of $-\text{div}\,(Q_R)$ imply that gas is emitting more radiation than it absorbs. Therefore, both the wide-band and the gray-gas models predict that the gas layer on the heating wall emits more radiation than it absorbs, and that the gas in the channel core absorbs more radiation than it emits. However, the gray-gas model does not predict that the gas layer on the insulated wall emits more radiation than it absorbs, while the wide-band model does predict it. This different feature of the results obtained by the gray-gas model from those by the wide-band model also appears in the case of black walls. In this case the wide-band model gives exact results since no reflection takes place at the black surfaces. Thus the gray-gas model has been found to be inadequate to estimate the net absorption $-\text{div}\,(Q_R)$, and the formulation using the wide-band model for non-black walls in this study can be reasonably stated to be valid for the case of thin optical thickness and high wall emissivities. In the case of low emissivities $\varepsilon = 0.18$, the corresponding profiles of $-\text{div}\,(Q_R)$ by the gray-gas model also differ from that by the wide-band model. The profile obtained by the wide-band model varies more sharply and gives larger absolute values in the vicinity of the walls than that by the gray-gas model. But at the insulated wall, differing from the case of high emissivities $\varepsilon = 0.82$, both the wide-band and the gray-gas models give positive values of $-\text{div}\,(Q_R)$. It is difficult to evaluate the validity of the proposed formulation from these results for the cases of low wall emissivities because radiation reflects at

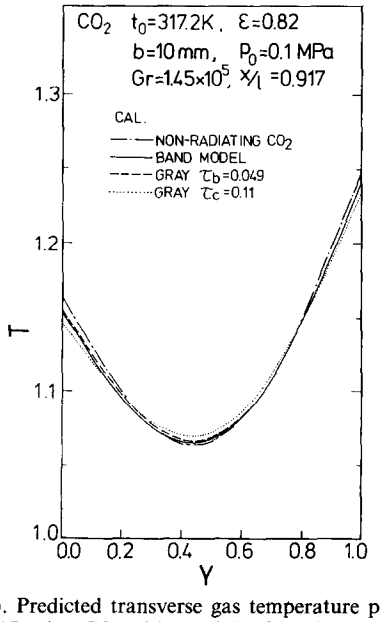

FIG. 8(a). Predicted transverse gas temperature profiles at $x/l = 0.917$ using CO_2 with $\varepsilon = 0.82$, $b = 10$ mm and $p_0 = 0.1$ MPa.

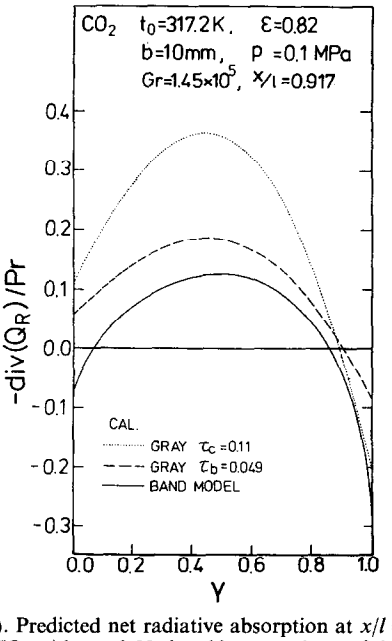

FIG. 8(b). Predicted net radiative absorption at $x/l = 0.917$ using CO_2 with $\varepsilon = 0.82$, $b = 10$ mm and $p_0 = 0.1$ MPa.

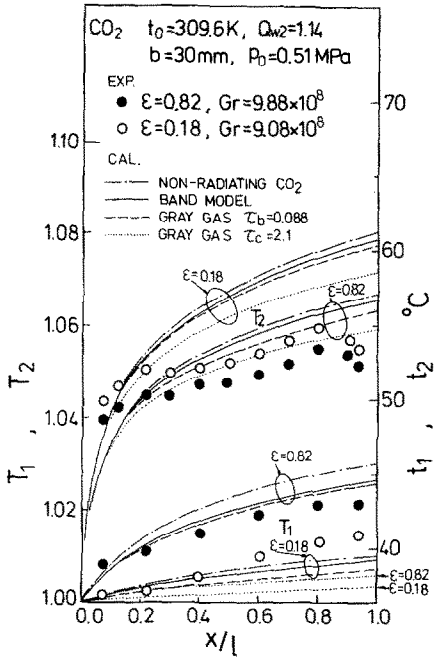

FIG. 9. Wall temperature profile in the flow direction for high and low emissivities using CO_2 with $b = 30$ mm and $p_0 = 0.5$ MPa.

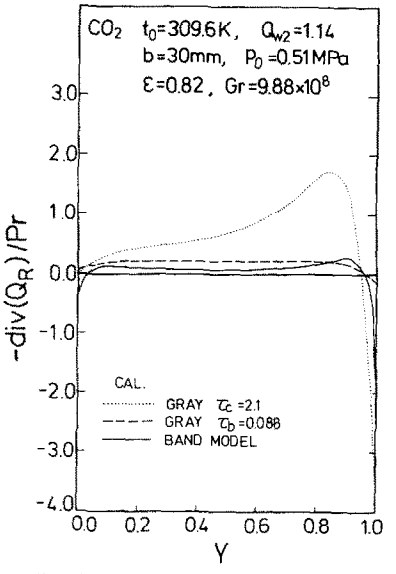

FIG. 10. Predicted net radiative absorption at $x/l = 0.940$ using CO_2 with $\varepsilon = 0.82$, $b = 30$ mm and $p_0 = 0.5$ MPa.

the walls many times to make the key assumption in this study doubtful. The validity should be evaluated by more accurate numerical calculations incorporating the narrow-band model, for example.

In order to obtain a more pronounced effect of gas radiation by making the optical depth thicker, the distance between the two surfaces was increased from 10 to 30 mm, and the pressure inside the vessel was raised from 0.1 to 0.5 MPa. Figure 9 shows the experimental and numerical results of the surface temperatures with the thicker optical depth. The wider channel width and the higher pressure increased the Grashof numbers, Gr, to the order of 10^8 which seemed to have resulted in transition from laminar to turbulent free convection. Therefore, sharp drops in the heating surface temperatures around $x/l = 0.3$ were observed, making the comparison of the numerical results with the experimental ones meaningless. In spite of this, the comparison between the numerical results will provide some information for the validity of the different models.

The temperature of the insulated surface predicted by the gray-gas model using $\tau_c = 2.10$ is unreasonably low compared with the other three curves. This is because the absorption coefficient given by equation (44) is valid only for a thin optical depth as mentioned before. The difference of the temperatures by the wide-band model and the gray-gas model using τ_b is now observable in Fig. 9, and it is seen that the gray-gas model using τ_b overestimates the gas radiation. The optical depth τ_b and the gas emissivity ε_g for this case are 0.088 and 0.150, respectively, and are about twice those for Fig. 6. However, $\tau_b = 0.088$ is still small and the gas radiation contribution is also small compared to the conduction contribution within the gas, thus satisfying the assumption employed in the formulation process. In addition, Soufiani and Taine [32] recently have compared the predictions by the exponential wide-band model with those by the statistical narrow-band model with the limited condition of black walls. They have found that in the optically thin limit, the wide-band model gave very close results to those of the narrow-band model. Their results give further verification of the analytical results predicted by the wide-band model in this study.

The net radiation absorption $-\mathrm{div}\,(Q_R)$ for the three models in Fig. 9 are also shown in Fig. 10. The gray-gas model using τ_c gives a highly deformed profile and very large absolute values of div (Q_R). The gray-gas model using τ_b predicts $-\mathrm{div}\,(Q_R)$ comparable to those by the wide-band model, but it again fails to predict the negative values in the thin layer next to the insulated wall. The Nusselt numbers Nu_2 at the heating surface for Fig. 9 were measured to be between 20 and 30. Even for these large Nusselt numbers, raising the surface emissivity from 0.18 to 0.82 has increased Nu_2 by about 15%.

5. CONCLUSIONS

By conducting analyses and experiments of combined radiation and free convection heat transfer in two-dimensional channels, the following has been concluded.

(1) A set of fundamental equations for combined heat transfer has been established which incorporates the exponential wide-band model with arbitrary surface emissivities.

(2) Numerical results of the surface temperatures

have agreed reasonably well with the experimental ones for cases using both radiating and non-radiating gas.

(3) The gray-gas model using two optical thicknesses has been compared with the wide-band model. Large errors in the surface temperatures and radiative fluxes have been found when using the optical thickness derived from the absorption coefficients at the thin limit. Even the optical thickness derived from the wide-band model has been found to have the tendency to overestimate the radiative transfer in the gas. The gray-gas model completely fails to predict the negative net radiation absorption in a thin layer next to the insulated wall.

(4) Even at a low temperature range between ambient and 150°C, surface radiation has dominant importance in the considered combined radiation and free convection with an asymmetric heating. Raising the surface emissivities from 0.18 to 0.82 increased the heat transfer coefficients at the heating surface by approximately 30%.

Acknowledgements—The author highly appreciates the valuable discussions with Professor K. Hijikata and Associate Professor T. Miyauchi at Tokyo Institute of Technology, and Dr M. Hirano at Mitsubishi Heavy Industry.

REFERENCES

1. R. Siegel and M. Perlmutter, Convective and radiant heat transfer for flow of a transparent gas in a tube with a gray wall, *Int. J. Heat Mass Transfer* **5**, 639–660 (1962).
2. E. G. Keshock and R. Siegel, Combined radiation and convection in an asymmetrically heated parallel plate flow channel, *J. Heat Transfer* **86**, 341–350 (1964).
3. Y. Mori, K. Hijikata and Y. Yamada, Radiation effects on heat transfer in the reactor core and heat exchangers of an HTGR, *J. Heat Transfer* **97**, 400–405 (1975).
4. Y. Mori, T. Taira and K. Watanabe, Heat exchanger augmentation by radiation plates, ASME Paper 76-HT-3 (1976).
5. Y. Yamada, M. Akai and Y. Mori, Shell-and-tube side heat transfer augmentation by the use of wall radiation in a crossflow shell-and-tube heat exchanger, *J. Heat Transfer* **106**, 735–742 (1984).
6. J. R. Carpenter, D. G. Briggs and V. Sernas, Combined radiation and developing laminar free convection between vertical flat plates with asymmetric heating, *J. Heat Transfer* **98**, 95–100 (1976).
7. R. Viskanta, Radiation heat transfer: interaction with conduction and convection and approximate methods in radiation, *Heat Transfer 1982. Proc. Seventh Int. Heat Transfer Conf.*, Munch, Vol. 1, pp. 103–121 (1982).
8. R. Viskanta, Radiative heat transfer, *Prog. Chem. Engng* **A22**, 51–81 (1984).
9. R. D. Cess, P. Mighdoll and S. N. Tiwari, Infrared radiative heat transfer in non-gray gases, *Int. J. Heat Mass Transfer* **10**, 1521–1532 (1967).
10. E. M. Sparrow, C. M. Usiskin and H. A. Hubbard, Radiation heat transfer in a spherical enclosure containing a participating heat-generating gas, *J. Heat Transfer* **83**, 199–206 (1961).
11. R. Viskanta, Interaction of heat by conduction, convection and radiation in radiating fluid, *J. Heat Transfer* **85**, 318–328 (1963).
12. M. Perlmutter and J. R. Howell, Radiant transfer through a gray gas between concentric cylinders using Monte Carlo, *J. Heat Transfer* **86**, 169–179 (1964).
13. H. C. Hottel and A. F. Sarofim, *Radiative Transfer*. McGraw-Hill, New York (1967).
14. T. H. Song and R. Viskanta, Development and application of a spectral-group model to radiation heat transfer, ASME Paper 86-WA/HT-36 (1986).
15. D. K. Edwards and W. A. Menard, Comparison of model for correlation of total band absorption, *Appl. Optics* **3**, 621–625 (1964).
16. C. L. Tien and J. E. Lowder, A correlation for total band absorption of radiating gases, *Int. J. Heat Mass Transfer* **9**, 698–701 (1966).
17. D. K. Edwards, L. K. Glassen, W. C. Hauser and J. S. Tuchscher, Radiation heat transfer in nonisothermal nongray gases, *J. Heat Transfer* **89**, 219–229 (1967).
18. R. M. Goody and M. J. S. Belton, Radiative relaxation times for Mars (a discussion of Martian atmospheric dynamics), *Planet. Space Sci.* **15**(2), 247–256 (1967).
19. D. K. Edwards and A. Balakrishnan, Slab band absorptance for molecular gas radiation, *J. Quant. Spectrosc. Radiat. Transfer* **12**, 1379–1387 (1972).
20. S. N. Tiwari, Applications of infrared band model correlations to nongray radiation, *Int. J. Heat Mass Transfer* **20**, 741–751 (1977).
21. S. DeSoto, Coupled radiation, conduction, and convection in entrance region flow, *Int. J. Heat Mass Transfer* **11**, 39–54 (1968).
22. I. S. Habib and R. Greif, Heat transfer to a flowing nongray radiating gas: an experimental and theoretical study, *Int. J. Heat Mass Transfer* **13**, 1571–1582 (1970).
23. R. Greif, Laminar convection with radiation: experimental and theoretical results, *Int. J. Heat Mass Transfer* **21**, 477–480 (1978).
24. M. Hirano, T. Miyauchi and Y. Mori, Enhancement of radiative heat transfer based on non-gray feature of radiative gas, *Proc. 8th Int. Heat Transfer Conf.*, Vol. 2, pp. 773–778 (1986).
25. D. K. Edwards and A. Balakrishnan, Nongray radiative transfer in a turbulent gas layer, *Int. J. Heat Mass Transfer* **16**, 1003–1015 (1973).
26. D. R. Jeng, E. J. Lee and K. J. Dewitt, A study of two limiting cases in convective and radiative heat transfer with non gray gases, *Int. J. Heat Mass Transfer* **19**, 589–596 (1976).
27. D. M. Kim and R. Viskanta, Interaction of convection and radiation heat transfer in high pressure and temperature steam, *Int. J. Heat Mass Transfer* **27**, 939–941 (1984).
28. Y. Takahira, Heat transfer analysis of flowing non-gray radiating gas, Report for Master's degree, Tokyo Institute of Technology (1987).
29. S. N. Tiwari and R. D. Cess, The effect of surface emissivity upon infrared gaseous radiation, *Int. J. Heat Mass Transfer* **11**, 1731–1734 (1968).
30. J. Gill and R. Goody, Convection in a radiating gas, *J. Fluid Mech.* **20**(1), 47–79 (1964).
31. L. Nichols, Temperature profile in the entrance region of an annular passage considering the effects of turbulent convection and radiation, *Int. J. Heat Mass Transfer* **8**, 589–607 (1965).
32. A. Soufiani and J. Taine, Application of statistical narrow-band model to coupled radiation and convection at high temperature, *Int. J. Heat Mass Transfer* **30**, 437–447 (1987).
33. J. Taine, A line by line calculation of low-resolution radiative properties of CO_2–CO-transparent nonisothermal gas mixtures up to 3000 K, *J. Quant. Spectrosc. Radiat. Transfer* **30**, 371–379 (1983).
34. J. M. Hartmann, R. Levi Di Leon and J. Taine, Line by line and narrow band statistical model calculations for H_2O, *J. Quant. Spectrosc. Radiat. Transfer* **32**, 119–127 (1984).
35. A. Soufiani, J. M. Hartmann and J. Taine, Validity of

band-model calculations for CO_2 and H_2O applied to radiative properties and conductive–radiative transfer, *J. Quant. Spectrosc. Radiat. Transfer* **33**, 243–257 (1985).
36. S. Fukusako and N. Seki, Simultaneous heat transfer by radiation and free convection from two-dimensional vertical parallel plates, *Proc. 5th Int. Heat Transfer Conf.*, Tokyo, Vol. 1(R2.11), pp. 113–117 (1974).
37. D. K. Edwards, Molecular gas band radiation. In *Advances in Heat Transfer*, Vol. 12, pp. 115–193. Academic Press, New York (1976).
38. W. Aung, L. S. Fletcher and V. Sernas, Developing laminar free convection between vertical flat plates with asymmetric heating, *Int. J. Heat Mass Transfer* **15**, 2293–2308 (1972).
39. D. K. Edwards and S. J. Morizumi, Scaling of vibration–rotation band parameters for nonhomogeneous gas radiation, *J. Quant. Spectrosc. Radiat. Transfer* **10**, 175–188 (1970).
40. R. D. Cess, The interaction of thermal radiation with conduction and convection heat transfer. In *Advances in Heat Transfer*, Vol. 1, pp. 1–50. Academic Press, New York (1964).
41. Y. S. Touloukian, D. P. DeWitt and R. S. Hernicz, *Thermal Radiative Properties, Metallic Elements and Alloys (Thermophysical Properties of Matter*, Vol. 7), p. 1218. IFI/Plenum, New York (1970).
42. Y. Yamada and M. Akai, Advanced high temperature gas heat exchanger, Tech. Report of Mech. Engng Lab., Japan No. 127 (1983) (in Japanese).

RAYONNEMENT CONJUGUE A LA CONVECTION THERMIQUE NATURELLE DANS UN CANAL VERTICAL AVEC DES EMISSIVITES ARBITRAIRES A LA PAROI

Résumé—On présente des études analytique et expérimentale du rayonnement combiné à la convection thermique naturelle dans un canal vertical, avec un milieu absorbant et émissif. Un canal entre plaques parallèles est chauffé dissymétriquement, ce qui rend important à la fois le rayonnement du gaz et celui des parois. Un système d'équations est établi en utilisant le modèle à bande exponentielle et le modèle de gaz gris, avec des émissivités de paroi arbitraires. Des résultats numériques sont comparés à ceux de l'expérience. Les émissivités de paroi ont un effet important sur le transfert de chaleur combiné. Le modèle de gaz gris est en défaut pour prédire l'absorption nette négative dans une couche de gaz proche d'une paroi isolée.

WÄRMEÜBERTRAGUNG DURCH STRAHLUNGSAUSTAUSCH UND FREIE KONVEKTION IN SENKRECHTEN KANÄLEN MIT BELIEBIGER EMISSIVITÄT DER WÄNDE

Zusammenfassung—Es wurden experimentelle und analytische Untersuchungen des kombinierten Wärmeübergangs durch Strahlung und freie Konvektion in einem senkrechten Kanal mit einem absorbierenden und ermittierenden Medium durchgeführt. Der Kanal besteht aus parallelen Platten, die asymmetrisch beheizt wurden, wobei sowohl Wand- als auch Gasstrahlung bedeutsam sind. Die grundlegenden Gleichungen für den Wärmeübergang wurden unter Verwendung des exponentiellen Breitband-Modells und des Grau-Gas-Modells bei beliebiger Wandemissivität formuliert. Die experimentellen und rechnerischen Ergebnisse wurden verglichen. Es ergab sich, daß die Wandemissivität einen wesentlichen Einfluß auf den kombinierten Wärmeübergang hat. Es konnte außerdem gezeigt werden, daß das Grau-Gas-Modell keine zuverlässigen Berechnungswerte liefert, sofern die Gasschicht nahe der isolierten Wände eine negative Strahlungsbilanz aufweist.

СОВМЕСТНЫЙ РАДИАЦИОННЫЙ И СВОБОДНОКОНВЕКТИВНЫЙ ТЕПЛООБМЕН В ВЕРТИКАЛБНОМ КАНАЛЕ С ПРОИЗВОЛЬНЫМИ ИЗЛУЧАТЕЛЬНЫМИ СПОСОБНОСТЯМИ СТЕНОК

Аннотация—Аналитически и экспериментально исследован совместный радиационный и свободноконвективный теплообмен в вертикальном канале в поглощающих и излучающих середах. Канал, образованный параллельными пластинами, нагревался асимметрично, причем существенными были излучения как стенки, так и газа. В рамках широкополосной модели и модели серого газа с произвольными излучательными способностями стенок выведена система основных уравнений. Сравнены численные и экспериментальные результаты. Найдено, что излучательная способность стенки оказывает определяющее влияние на комбиниорованный теплоперенос. Показано, что модель серога газа не позволяет получить суммарное отрицательное поглощение в слое газа вблизи теплоизолированной стенки.